Journal of Science: Advanced Materials and Devices 4 (2019) 80–88

Contents lists available at ScienceDirect

Journal of Science: Advanced Materials and Devices

journal homepage: www.elsevier.com/locate/jsamd

Original Article

The TiO_2-graphene oxide-Hemin ternary hybrid composite material as an efficient heterogeneous catalyst for the degradation of organic contaminants

C. Munikrishnappa [a, d, *], Surender Kumar [b], S. Shivakumara [c], G. Mohan Rao [a], N. Munichandraiah [d]

[a] Department of Instrumentation and Applied Physics, Indian Institute of Science, Bangalore, 560012, India
[b] CSIR - Advanced Materials and Processes Research Institute, Bhopal, 462026, India
[c] School of Chemical Sciences, REVA University, Bangalore, Karnataka, 560064, India
[d] Department of Inorganic and Physical Chemistry, Indian Institute of Science, Bangalore, 560012, India

ARTICLE INFO

Article history:
Received 28 June 2018
Received in revised form
14 December 2018
Accepted 16 December 2018
Available online 27 December 2018

Keywords:
Photocatalysis
Advance oxidation processes (AOPs)
Metal ligand charge transfer processes (MLCTs)
Rhodamine B

ABSTRACT

TiO_2-Graphene Oxide-Hemin (TiO_2/GO/Hemin) ternary composite hybrid material was prepared by the sol-gel method and used as a heterogeneous catalyst for the photocatalytic degradation of organic contaminants. The catalytic activity of GO-TiO_2-Hemin was evaluated by the degradation of Rhodamine B (RhB) under the UV-visible light irradiation and in the presence of hydrogen peroxide. The ternary composite of (TiO_2/GO/Hemin) shows an excellent activity over a wide pH range from 3 to 11 and also a stable catalytic activity after five recycles. The increase in the efficiency of TiO_2-GO-Hemin-UV processes is attributed to the Fe^{2+} ions produced from the cleavage of stable iron complexes, which participate in the continuous cyclic process for the generation of hydroxyl radicals resulting from the heterogeneous photocatalytic reactions and the adsorption power of GO.

1. Introduction

Nowadays, wastewater is a great challenge for all societies, mostly caused by organic pollutants [1]. Organic dyes being used in industries have been identified as one of environment hazardous chemical wastes. Therefore, there is an urgent need of removal of organic dyes from the polluted waste water [2]. To control the water pollution, various technologies have been developed, including physical, chemical, biological, and electrochemical methods [3,4]. Among the available technologies, the advanced oxidation processes (AOPs) have emerged as one of the promising alternative strategies for the effluent treatment and decontamination of water. AOPs have their own unique advantages including a high photocatalytic efficiency, the environmental benign nature, low cost, safe application and a mass scale accessibility. AOPs are characterized by the capability of exploiting the high reactivity of hydroxyl radicals in driving oxidation processes [5,6]. Hydroxyl radicals have very high oxidizing power, and are able to degrade organic hazardous dyes. It has a potential of resolving the energy crisis as well. However, the traditional Fenton system requires highly acidic conditions to avoid the Fe^{2+} and Fe^{3+} hydrolysis. Moreover, the removal of the sludge containing iron ions complicates the process and makes the method expensive [7,8]. To overcome these disadvantages of the homogeneous Fenton process, there is the demand for a heterogeneous catalyst including iron-containing materials [9].

Graphene, an attractive carbon material, has gained great attention due to its excellent electronic properties and great application potential [10]. Graphene is being widely used as an active support for the detection and treatment of wastewater [11]. Graphene based hybrid materials are prepared by using graphene oxide (GO), which contains various oxygen functionalities on the surface. Functional groups on GO are favourable for the immobilization of metals, biomolecules, drugs and inorganic nanoparticles [12]. Compared to graphene, GO has attracted due to a

* Corresponding author. Department of Instrumentation and Applied Physics, Indian Institute of Science, Bangalore, 560012, India.
E-mail address: ipcmunikrishna@gmail.com (C. Munikrishnappa).
Peer review under responsibility of Vietnam National University, Hanoi.

https://doi.org/10.1016/j.jsamd.2018.12.003

great deal of its easy availability, environmentally benign nature, chemical functionalization, good dispersion in water and high biocompatibility [13]. It also has been found that the graphene oxide composite generates electron-hole pairs while decomposing the pollutants. Most of the industrial pollutants are aromatics in nature, and they get adsorbed with reduced graphene through the π-π interactions. This adsorption process significantly increases the concentration of the organic pollutant molecules near the catalytic surface. The enriched environment of the substances very closed to the catalytic surface is an important factor contributing to the higher photocatalytic activity.

Titanium dioxide (TiO_2) is one of the conspicuous materials as photocatalyst in the field of environmental applications. TiO_2 is used as one hybrid component coupled with many semiconductors like TiO_2–SnO_2, TiO_2–ZnO TiO_2-RGO *etc*. For better performance, the composite of TiO_2 and reduced graphene oxide is another good photocatalyst for organic pollutants [14,15].

Hemin is an active center of heme-proteins, such as cytochromes, peroxidases, myoglobins and hemoglobins, which has peroxidase like activity. Hemin enables a free radical mechanism induced by the addition of H_2O_2, which leads to the formation of covalent bonds between the halogenated phenols and humid substances [16]. However, the catalytic coupling reaction is studied in UV-visible irradiation, thus implying a contribution of photo-oxidation to the Rhodamine B (RhB) dye.

In the present work, the photocatalytic degradation of Rhodamine B (RhB) is investigated by using the ternary composite TiO_2/GO/Hemin as a photocatalyst. The degradation process is further studied by spectroscopic techniques, such as High Performance Liquid Chromatography (HPLC) and Liquid Chromatography Mass Spectrometry (LCMS). Probable degradation mechanism of RhB is proposed based on intermediates.

2. Experimental

2.1. Materials

Titanium (IV) chloride ($TiCl_4$), Rhodamine B, Acetonitrile (HPLC grade), Hydrogen peroxide (30% w/v), Graphite powder (Graphite India) $NaNO_3$, $KMnO_4$ and Dimethyl sulfoxide (SD Fine Chemicals), and Hemin (Sigma Aldrich) were used as starting materials. All the chemicals were of analytical grade and used as received. Double distilled water was used for all experiments.

2.2. Preparation of graphene oxide (GO)

For the preparation of GO, graphite powder was first converted into graphite oxide using the procedure described by Hummers and Offeman [17]. In brief, graphite powder (3.0 g) was added to 69 ml of concentrated H_2SO_4 with 1.50 g $NaNO_3$ dissolved in it. The mixture was stirred for 1 h at ambient temperature. The container was cooled in an ice bath, and 9.0 g $KMnO_4$ was slowly added while vigorously stirring the contents by a magnetic stirrer for about 15 min. Two aliquots of 138 ml and 420 ml double distilled water were slowly and carefully added in about 15 min intervals. Subsequently, 30% H_2O_2 was added and the color of the suspension changed from light yellow to brown indicating the oxidation of graphite. The product of graphite oxide was separated by centrifugation, then washed with warm water and ethanol several times, and finally dried at 50 °C for 12 h. Graphite oxide (100 mg) was transferred into 600 ml double distilled water and sonicated for 3 h. The graphite oxide was exfoliated to graphene oxide by sonication, which was separated by centrifugation, washed with double distilled water and ethanol, followed by drying at 50 °C for 12 h.

2.3. Preparation of TiO_2/Graphene oxide/Hemin composite

Anatase TiO_2 nanoparticles were synthesized by a sol-gel technique [18]. For the preparation of the hybrid composite material, 25 mg GO was dispersed in 20 ml ethanol using sonication to form a colloidal suspension. 75 mg of TiO_2 was added to the GO solution to get the desired dopant concentration of GO. This mixture was ground in a mortar and dried in oven at 50 °C for 3 h. The process of grinding was repeated for five times, and the resulting product was dried in a vacuum oven at 50 °C for 24 h.

Accurately weighed TiO_2/GO was immersed in the freshly prepared Hemin solution made up of 1:1 ratio of dimethylsulfoxide and acetonitrile (DMSO/CH_3CN), at acidic pH for 24 h, and then centrifuged to remove the solvent. The resulting TiO_2/GO/Hemin composite was dried at room temperature.

2.4. Physico-chemical characterization

The powder X-ray diffraction (PXRD) patterns were recorded using a Philips 'X' PERT PRO diffractometer with Cu-Kα radiation ($\lambda = 1.5438$ Å) with a Ni filter as the X-ray source. The diffraction patterns were recorded at room temperature in two theta range 10–80° at a scan rate of two degree per min. Fourier Transform InfraRed (FTIR) spectra of synthesized catalysts were recorded on a 1000 Perkin–Elmer FTIR spectrometer in the range of 400–4000 cm^{-1}. To study the light absorption characteristics of the photocatalysts, the UV-visible absorption spectra were recorded using the Shimadzu UV-3101 PC UV-VIS-NIR UV-Visible spectrophotometer in the range 200–800 nm. The electrochemical measurements were performed using PARCEG & G potentiostat/galvanostat mode versastat II in a three-electrode system with the semiconductor working electrode, a Pt foil and a standard calomel electrode (SCE) as the working, the counter and the reference electrode, respectively. Further, for the identification of the oxidized products of Rhodamine B (RhB) the liquid chromatography mass spectroscopy (LCMS), Thermo, and LCQ Deca XP MAX LC-MS analysis were used.

2.5. Photocatalytic degradation procedure

AOPs were performed in a Pyrex glass reactor (150 × 75 mm) with a surface area of 176 cm^2. The experimental design constitutes of an 125 W high pressure mercury vapor lamp, whose photon flux is 7.75 mW/cm^2 as determined by the Ferri Oxalate actinometry, and the wavelength of it peaks in the range 500–600 nm. The light source is made to focus directly on the reactor, and the distance between the lamp housing and the reactor is 29 cm. In a typical experiment, 250 ml of the 10 ppm dye solution along with the desired amount of photocatalyst was added into the reaction solution. The lamp was warmed for 5 min to reach constant output and then the oxidant was added. The electro-chemical deposition was carried out by the potentiodynamic method on the fluorine doped tin oxide (FTO)-coated glass electrodes. The FTO electrodes were well cleaned by sonication for 15–30 min consecutively in water, acetone and isopropanol. Subsequently, they were dried in the N_2 flow and stored under vacuum at room temperature.

The pH of the solution was measured at the beginning and at the end of each experiment.

3. Results and discussion

3.1. Powder XRD

The powder XRD patterns of the samples of TiO_2, GO, TiO_2/GO, TiO_2/Hemin, and TiO_2/GO/Hemin composite are shown in Fig. 1. The

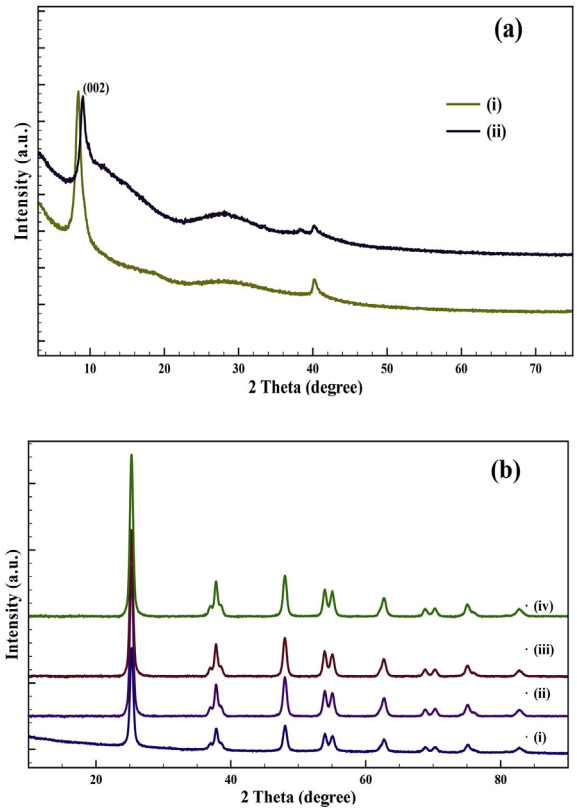

Fig. 1. (a) Powder XRD pattern of graphite oxide (i), graphene oxide (ii), and (b) (ii) TiO_2, (ii) TiO_2/GO, (iii) TiO_2/Hemin, (iv) TiO_2/GO/Hemin.

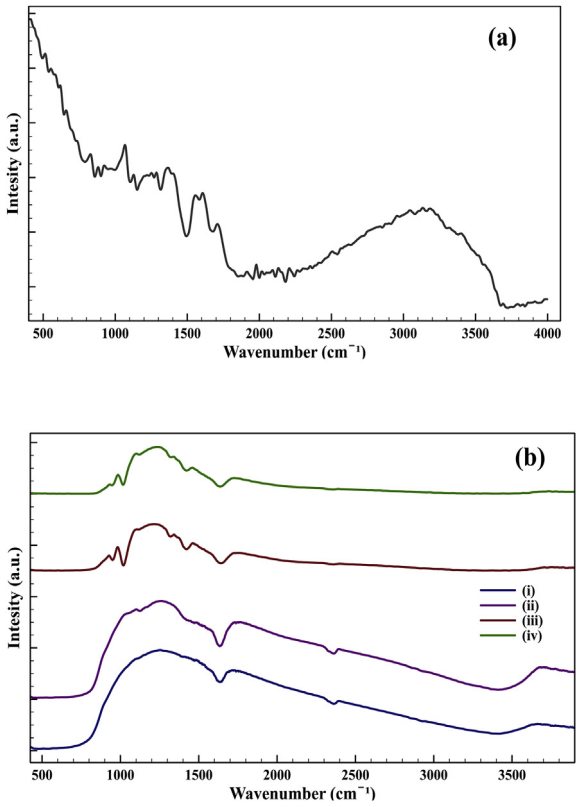

Fig. 2. FTIR pattern of (a) graphene oxide, and (b) TiO_2 (i), TiO_2/GO (ii), TiO_2/Hemin (iii), TiO_2/GO/Hemin (iv).

pattern of the anatase TiO_2 exhibits peaks at 2θ values of 25.30 (101), 38.57 (112), 48.04 (200), 53.88 (105), 55.07 (211), 62.69 (204) and 68.75 (116). Graphite (Fig. 1a (i)) is characterized by the strong (002) reflection at 26.51 corresponding to the hexagonal graphitic structure. The interlayer distance of the (002) reflection obtained from graphite is 3.38 Å. This is comparable with the reported values [19]. In the pattern of GO, the (002) reflection is shifted to 10.31 (Fig. 1a (i) (ii)). This value corresponds to an interlayer distance of 8.48 Å, indicating the expansion of graphite due to the presence of the oxygen containing functional groups on both the sides of the graphene sheets and also due to the atomic scale toughness because of the sp^3 bonding in carbon. There is a shift in the (002) reflection of graphite oxide, indicating the conversion of graphene oxide to graphite oxide. XRD patterns of the TiO_2, GO, TiO_2/GO, TiO_2/Hemin, and TiO_2/GO/Hemin peaks corresponding to the anatase phase at 2θ values of 25.30 (101), 38.57 (112), 48.04 (200), 53.88 (105), 55.07 (211), 62.69 (204) and 68.75 (116) (JCPDS, FILE NO.21–1272) along with the respective crystal planes of anatase phases are shown in (Fig. 1b).

3.2. FTIR spectra

FTIR spectra of TiO_2, GO, TiO_2/GO, TiO/Hemin, and TiO_2/GO/Hemin are represented in Fig. 2b. TiO_2 shows strong and broad characteristic absorption peaks at 3399 cm^{-1} and 1635 cm^{-1}, which can be attributed to the stretching and bending modes of vibration of adsorbed water and hydroxyl groups, respectively (Fig. 2b). FTIR spectral analysis of the functionalized GO and TiO_2/GO are shown in Fig. 2a. This important observation revealed that the band at 3620 cm^{-1}present in the spectrum of GO originated from the stretching of the O–H bond on the GO surface. The bands at 1709, 1584, 1222 and 1039 cm^{-1} are assigned to the C=O, C=C, C–OH and C–O stretching vibrations, respectively. The IR spectra of the TiO_2/Hemin show a highly intense band at 1019 cm^{-1}, due to the C–O stretching vibration and a split peak around 1435-1400 cm^{-1}, corresponding to the C=O vibrations of the surface bound carboxylic acid and the hydrogen bonded carboxylic acid, and another small peak appears at 1317 cm^{-1} due to C–O, respectively. FTIR characterization confirms the binding of the Hemin porphyrin complex to the TiO_2/GO surface through the O=C–O–Ti bond [Scheme 1]. The strong band in the range of 400–900 cm^{-1} corresponds to the stretching vibrations of the Ti–O–Ti bond [20].

3.3. TEM analysis

Fig. 3 (a) and (b), respectively, show the Transmission Electron Microsopy (TEM) images of the GO and the TiO_2/GO/Hemin. It is clear that in the synthesized catalysts there is a direct interaction between the TiO_2 nanoparticles, the Hemin molecule and the graphene oxide sheets, and that interaction prevents the reaggregation of the graphene oxide sheets. The TEM images also provide an easy

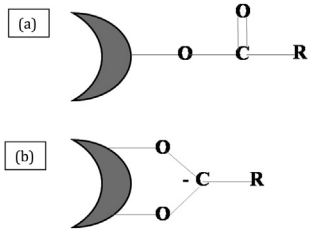

Scheme 1. (a) Uncomplexed carboxylic acid linkage and (b) complexed carboxylate linkage.

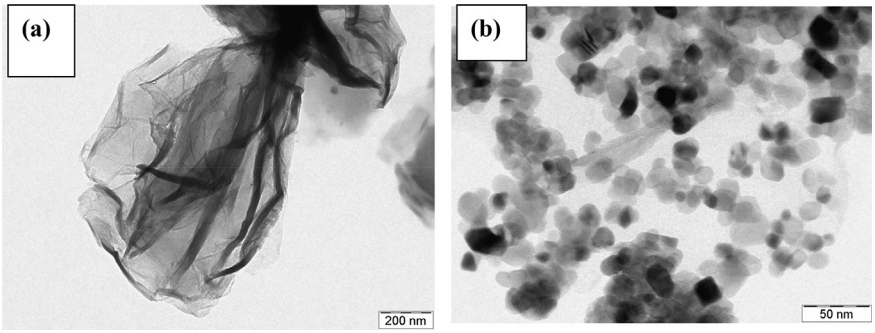

Fig. 3. TEM image of GO (a), and TiO_2-GO-Hemin (b).

distinction of TiO_2/GO and Hemin molecules with lighter and darker shades. The Hemin molecules are highly dispersed on the surface of GO and are bound of the TiO_2 particles with a distinguishable grain boundary.

3.4. LCMS characterization

The LCMS experiment was used to characterize the formation of thintermediates during the photocatalysis with TiO_2/GO/Hemin/UV. The sample before the UV irradiation shows an m/z peak at 443 of a high intensity corresponding to the parent dye molecule. The parent molecule structure of these intermediates was then identified by the LCMS, HPLC and UV visible spectrophotometry. The main intermediates corresponding to the m/z values are summarized in Table 1. The RhB dye molecules lost the ethyl groups step by step to transform to the products as $DMRh^+$, DRh^+, $MMRh^+$, MRh^+ and Rh^+, and the final mineralization of CO_2 and H_2O. The adsorption modes of the RhB on the surface of TiO_2/GO/Hemin greatly influence the photocatalytic degradation mechanism of the RhB as shown in LCMS mechanism [Scheme 2]. Our results indicate that the photo-oxidation process, the major active oxygen species and the hydroxyl groups attacking at the RhB dye are highly selective. The proposed reaction mechanism can be considered as an evidence supporting the suggestion that hydroxyl radicals and the active oxygen species are responsible for the chromophore destruction [21].

3.5. Photoelectrochemical studies

Photoelectrochemical studies were carried out using TiO_2, TiO_2/GO,TiO_2/Hemin and TiO_2/GO/Hemin samples under the UV light illumination (Fig. 4). The life time stability of the photocatalytic efficiency of the photocatalysts was elucidated with the transient photocurrent generation of charges. The photocatalytic activity is dependent on the efficiency of current. The higher the current, the higher will be the photocatalytic activity. The observed photocurrent magnitude is higher for the TiO_2/GO/Hemin under the UV light irradiation compared to that for the TiO_2, TiO_2/GO and TiO_2/Hemin. The observed photocurrent for TiO_2/GO/Hemin under the UV light is due to the charge transfer process from the excited hemin moiety to the CB of TiO_2, TiO_2/GO and TiO_2/Hemin. The transient photocurrent density of TiO_2/GO/Hemin is much higher than that of the TiO_2, TiO_2/GO,TiO_2/Hemin and that is highly reproducible in numerous on/off cycles under the light on and light off conditions. These electrons are expected to move in the external circuit to generate the photocurrent. The magnitude of the photocurrent was tested for several light on and off cycles repetitions and it was observed to be constant, determining the separation efficiency of the catalyst in the reaction medium [22].

Table 1
Degraded products of LCMS.

S. No.	Retention time, RT	Corresponding intermediates of RhB Compound	Mass (m/z)
1	13.3	Rhodamine B (RhB+)	443.3
2	8.4	($DMRh^+$)	415.2
3	5.6	DRh+	387.2
4	5.6	MMRh+	387.2
5	4.5	MRh+	359.3
6	3.8	Rh+	331.2

3.6. Recycling studies

Recycling reactions were used to evaluate the photo stability and reusability of the TiO_2, TiO_2/GO, TiO_2/Hemin, and TiO_2/GO/Hemin samples. As shown in Fig. 5, five consecutive values of the degradation rates of TiO_2, TiO_2/GO,TiO_2/Hemin and TiO_2/GO/Hemin samples are found to decrease from 96.45%(1st) to 90.72% (5th). The photocatalytic efficiency was only slightly lower, considering the loss of catalysts in each cycling process and the test error. At the end of each experiment the catalyst particles were washed thoroughly and air dried. The experimental results imply that the materials have great potential and are photostable with a good reusability for the promising practical applications.

3.7. Effect of the initial dye concentration

The degradation efficiency depends on the initial concentration of the substrate. The effect of the concentration on the degradation of the RhB dye was studied in the concentration ran from 10 ppm to 100 ppm. The influence of the initial dye concentration on the rate of degradation were performed at different initial dye concentrations while keeping the other parameters constant. As the initial dye concentration increases, the rate of degradation decreases, due to the non-availability of a sufficient number of hydroxyl radicals and also due to the impermeability of the UV rays [23]. Several factors like dye concentrations serve as an inner filter for shunting the photons away from the catalyst surface, the collision probability between the dyes and the decrease in oxidising species can also account for the decrease in the degradation rate. Another important reason could be assigned to the adsorption and oxidation of more dye molecules on the catalyst surface covering the catalytic active sites which are required to absorb the photons, and hence, decreasing the overall rate of degradation. It was found that the efficiency was maximum for the 10 ppm concentration. Therefore, it is desirable to have lower initial dye concentrations for the effective degradation by AOPs (Fig. 6).

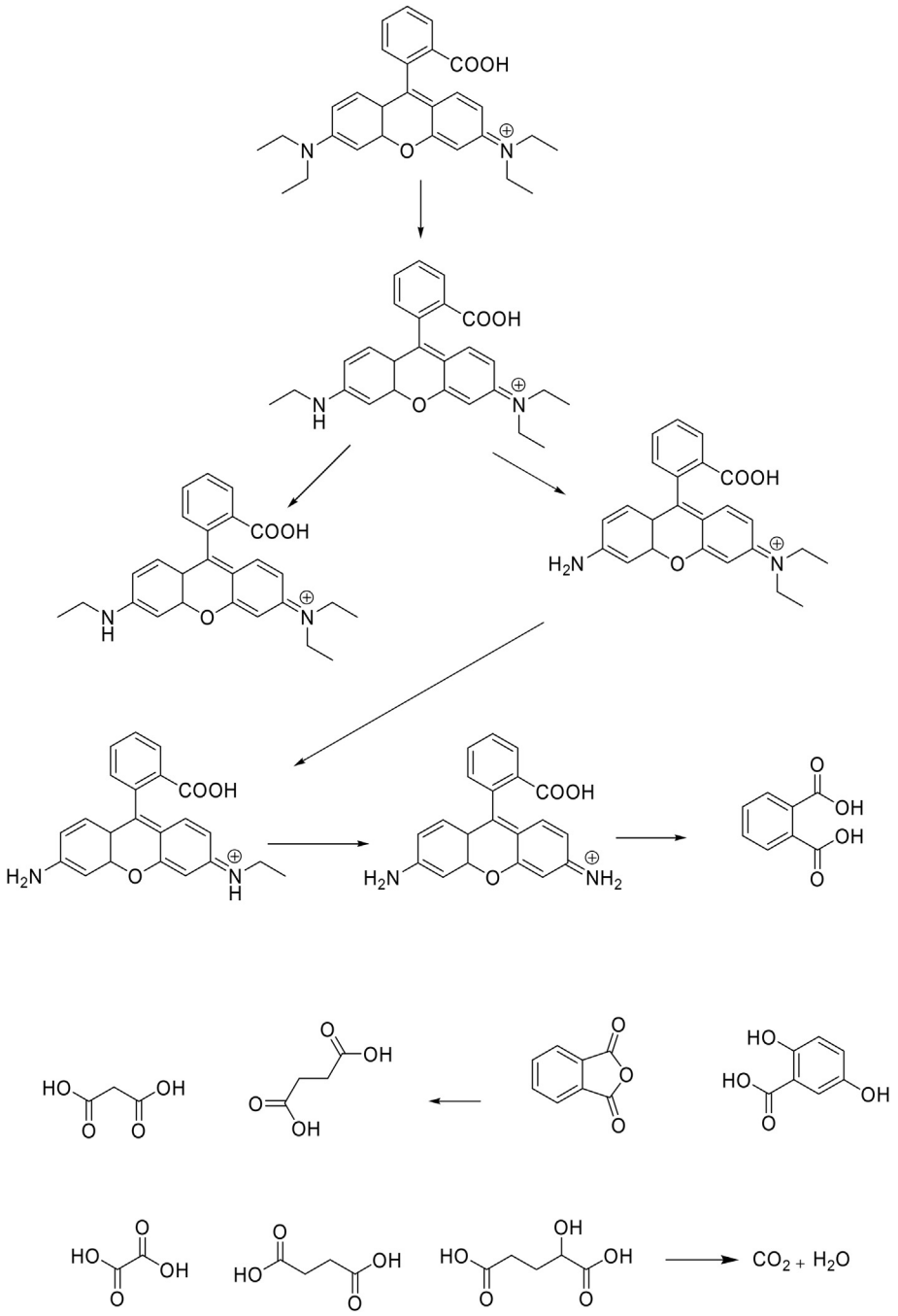

Scheme 2. The probable degradation mechanism of LCMS technique for RhB.

3.8. Effect of pH

The experimental results show that the Hemin catalyst has an excellent photocatalytic activity in pH which tolerates over a wide pH range from 3 to 11. The rate of degradation and percentage of degradation of RhB were observed to be constant irrespective of the pH value for the given reaction conditions. As reported earlier in the literature, most of the Fenton reactions are effective only at pH = 3, when Fe^{3+}/Fe^{2+} or Fe^0 was used as catalyst along with H_2O_2. Lower or higher pH conditions resulted in the precipitation of iron as iron oxyhydroxide and in the appearance of turbidity in the reaction mixture. In case of Hemin, pH restrictions were not found, and the system is varied in a wide pH range from pH 3 to 11. This is an important result showing the efficiency of the photocatalytic process where Hemin can be used under all pH conditions.

3.9. Effect of the oxidants on the degradation of RhB

The oxidizing agents enhance the production of hydroxyl radicals under the UV irradiation and affect to improving the photocatalytic degradation of the RhB dye. Hydroxyl radicals originate from either the excited holes in the valence band of the semiconductor or the oxidant accepting electron in the conduction band of the semiconductor, thereby these oxidants increase the number of the trapped electrons, which prevents electron − hole recombination and generates oxidizing species, to increase the oxidation

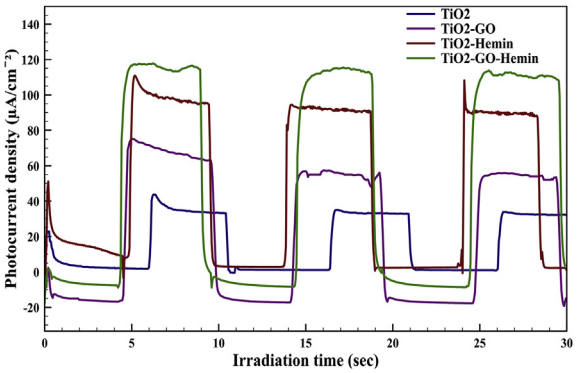

Fig. 4. Transient photocurrent responses of photocatalysts.

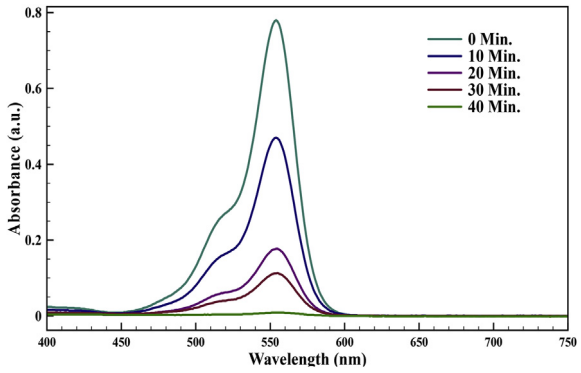

Fig. 6. The plot of concentration of RhB dye versus time under UV illumination for various Degradation processes.

rate of the intermediate compounds. H_2O_2 is more electropositive than free O_2, implying that H_2O_2 is a better electron acceptor than the molecular oxygen that ultimately leads to CO_2. The reactions taking place when H_2O_2 is present in the TiO_2 suspension can be represented by the following equations [24].

$$H_2O_2 + h^+ \rightarrow HO_2 + H^+ \quad (1)$$

$$H_2O_2 + HO \rightarrow HO_2 + H_2O \quad (2)$$

$$HO_2 + HO \rightarrow H_2O + O_2 \quad (3)$$

However, when H_2O_2 is added to the TiO_2/GO/Hemin system, there is a significant enhancement in the rate of the photocatalytic degradation. The efficiency of the various processes for the degradation of the RhB dye is of the following order: GO/H_2O_2< TiO_2/H_2O_2<Hemin/H_2O_2<TiO_2/GO/H_2O_2<TiO_2/Hemin/H_2O_2<TiO_2/GO/Hemin/H_2O.

3.10. Kinetic study and the process efficiency

The kinetic studies of the degradation for all the above oxidation processes are summarized and presented in Table 2. The degradation in the presence of TiO_2/GO/Hemin/H_2O_2/UV may be attributed to the formation of Hemin complexes between the iron ions and the dye molecules preferably with the chromophore of the RhB [Scheme 3]. The generation of the hydroxyl radicals via the photolysis of H_2O_2 and the degradation of the dye molecules through the direct photolysis additionally contribute to the overall enhancement in the mineralization. The calculation of the apparent

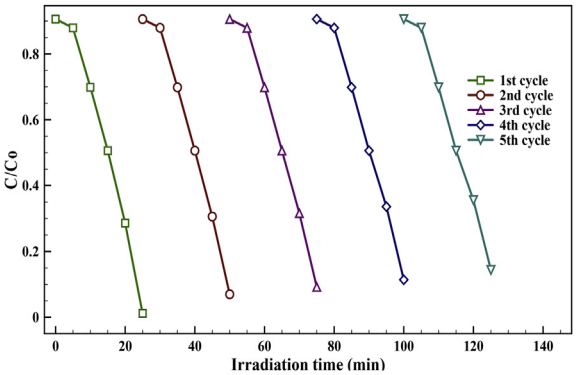

Fig. 5. Recyclable photodegradation of the photocatalyst TiO_2/GO/Hemin for 1st to 5th cycle.

first order constant '*k*' for the RhB degradation by the above mentioned processes was studied for the time period of 40 min. The results suggest that Hemin is an efficient catalyst and can be used in the heterogeneous photocatalysis. The process efficiency (Φ) in all the above cases can be defined as the change in the concentration by the amount of energy in terms of the intensity and the exposure surface area per time.

$$\Phi = \frac{(C_0 - C)}{t.I.S} \quad (4)$$

In the equation above, C_0 is the initial concentration of the substrate and *C* is the concentration at time'*t*'; (C_0–C) denotes the residual dye concentration in mg/liter or ppm; '*I*' is the irradiation intensity 125 W; '*S*' denotes the solution irradiated plane surface area in cm^2 and '*t*' represents the irradiation time in minutes.

The process efficiency calculated from the various processes are given in Table 2. It is observed that the process efficiency is highest for the system of TiO_2/GO/Hemin/H_2O_2. From the kinetics data the extent of the degradation with the various systems is presented in the following order: GO/H_2O_2<TiO_2/H_2O_2<Hemin/H_2O_2<TiO_2/GO/H_2O_2<TiO_2/Hemin/H_2O_2<TiO_2/GO/Hemin/H_2O_2 (Fig. 7).

3.11. Comparison of the photocatalysts

The Rhodamine B dye is indeed a pollutant but it is extensively used in the textile and leather industry. However, the existence of this hazardous dye in the water causes serious health problems. It is therefore necessary to remove the RhB from the wastewater so that it can be reused. For the removal of RhB and mineralization, the composite of Titania, Graphene Oxide and the Hemin ternary hybrid nanoparticle semiconductor photocatalyst was investigated. Photocatalytic experiments were conducted on the samples with the definite dye concentration (10 ppm) in an attempt to compare the efficiency of the various photocatalysts. The concentration of the RhB dye is considered as the sink of the linear part of the absorbance–desorbance curve (Beer's Law). The ternary composite (TiO_2/GO/Hemin) was found to show the highest photocatalytic activity. The reduction in the electron and hole recombination due to the separation of the photogenerated electrons on the conduction band of TiO_2 that can transfer to the graphene oxide. Because the Fermi energy of graphene is much lower than the conduction band of TiO_2, the graphene can act as a sink for the photo generated electrons. The excited electrons can be stored in the huge π–π interaction of graphene oxide in the composite, which can retard the photogenerated electron hole recombination on TiO_2. This process facilitates the effective interface charge separation and hinders the carrier recombination. The electron transfer between

Table 2
Rate constant and process efficiency calculated for various oxidation processes on the degradation of RhB.

Oxidation processes system	Processes efficiency $\times 10^{-6}$ ppm $min^{-1}W^{-1}cm^{-2}$	Rate constant $\times 10^{-3}$ min^{-1}	Time in minutes	% Degradation
$TiO_2 + H_2O_2$	0.25	0.25	180	10
$GO + H_2O_2$	0.22	0.20	180	9
$Hemin + H_2O_2$	3.80	4.40	120	100
$TiO_2 + GO + H_2O_2$	5.71	7.10	80	100
$TiO_2 + Hemin + H_2O_2$	7.72	9.60	60	100
$TiO_2 + GO + Hemin + H_2O_2$	11.51	14.7	40	100

TiO_2 and graphene oxide nanoparticles is expressed in Eqs. (5) and (6).

$$TiO_2 + h\gamma \rightarrow e^-(CB\ TiO_2) + h^+(VB\ TiO_2) \quad (5)$$

$$GO + e^-(CB\ TiO_2) \rightarrow e^-(GO) + TiO_2 \quad (6)$$

This proposes a reaction mechanism involving the dechlorination of the alkyl halides (R-X), with X = Cl which occurred via the abstraction of the chlorine atom by the Fe^{2+}centre in the Hemin molecule to form the Fe^{3+} complex along with the formation of the free radicals and this mechanism is referred to as the inner sphere electron transfer mechanism [25,26]. Such inner sphere electrons transfer mechanism can be proposed in the present case for the degradation of the RhB in the following way:

$$Fe^{II} + RhB \leftrightarrow Fe^{II}(RhB) \rightarrow [Fe\cdots RhB]^{\neq} \rightarrow Fe^{III} - RhB\ complex + Free\ radicals \quad (7)$$

Or

$$Fe^{II} + RhB \rightarrow Fe^{III} + Degradation\ products \quad (8)$$

Alternatively, the dehalogenation of polyhalomethanes and ethanes (including CCl_3R where R = H, Cl, $CHCl_2$, CCl_3, and CH_3) in the presence of an iron (II) porphyrin (meso-tetrakis[*N*-methylpyridyl] iron porphyrin) and the cysteine was studied. The authors proposed an outer-sphere electron transfer, in which as the first step an electron was transferred to the halogenated alkanes (R-X), followed by either the generation of a carbanion $[R\text{-}X]^-$ or the dissociation of the weakest carbon-halogen bond or both. If one proposes this outer sphere electron mechanism for the degradation of the RhB, a free radical anion of the RhB is formed from the electron obtained by the Hemin molecule [27].

$$RhB + e^-\ (from\ Hemin) \rightarrow [RhB]^- \rightarrow Free\ radical + ion \quad (9)$$

Alternatively, the authors in Ref. [28] proposed a cyclic mechanism in which iron has the +3 oxidation state $[HOFe^{III}\text{-}L]$ and forms a peroxo complex of the type $[HOOFe^{III}\text{-}L]$ in the presence of H_2O_2. This complex, under the UV-visible light irradiation, forms the high-valence iron-oxo species of the type $[\cdot OH\cdots O{=}Fe^{IV}\text{-}L]$ [27]. This complex reacts with substrate to regenerate the $[HOFe^{III}\text{-}L]$. This cyclic process continuously sustains the degradation reaction. This type of oxo species is formed by the metal ligand charge transfer (MLCT) process along with the active hydroxyl radical, which was shown to positively enhance the degradation rate immensely. The authors have used cyclodextrin as an extremely attractive component of an artificial enzyme and the attachment of this simple hemicatalytic group to this cyclodextrin affords the interesting enzyme mimics. Although the cyclodextrin is not used in this study, such complex formation cannot be ruled out completely and the presence of iron in a higher oxidation state is yet to be explored. However, the active involvement of the hydroxyl radicals were explored by performing the degradation reaction. The results showed that the hydroxyl radicals were actively participating in the degradation mechanism. The OH free radicals generated in the present case predominantly react with the substrate RhB molecules and degrade them effectively. The electron transfer from the excited state of Hemin to the conduction band of TiO_2 is thermodynamically favorable, as the oxidation potential of the excited state of Hemin is higher than the conduction band energy level of TiO_2 [29], and the continuous photo irradiation absorption of the TiO_2/GO electrons occurs, which absorbs light throughout the experimental conditions. Valence band holes are known to reversibly oxidize to carboxylates that allow the concentration of

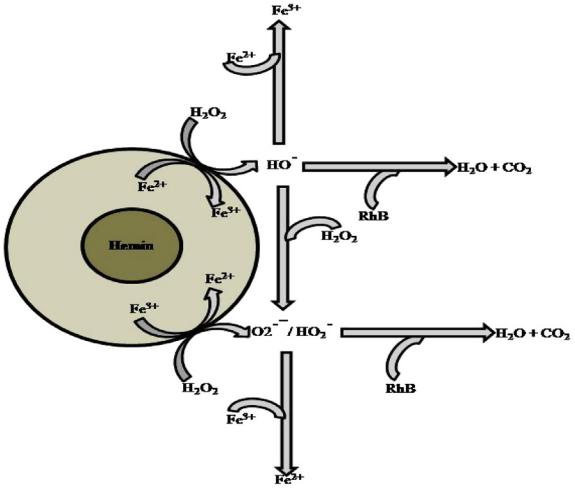

Scheme 3. Schematic representation of the proposed reaction mechanism.

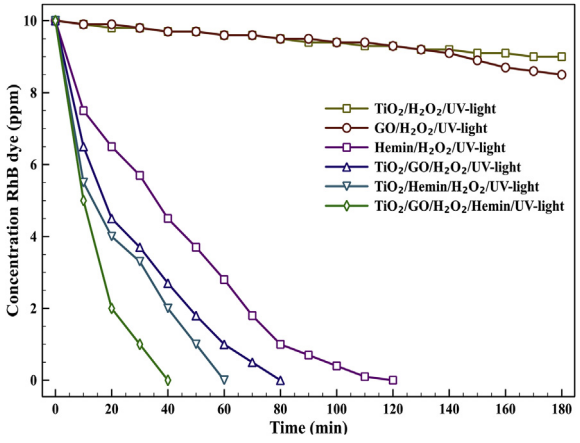

Fig. 7. Percentage degradation of the RhB dye for different oxidation processes.

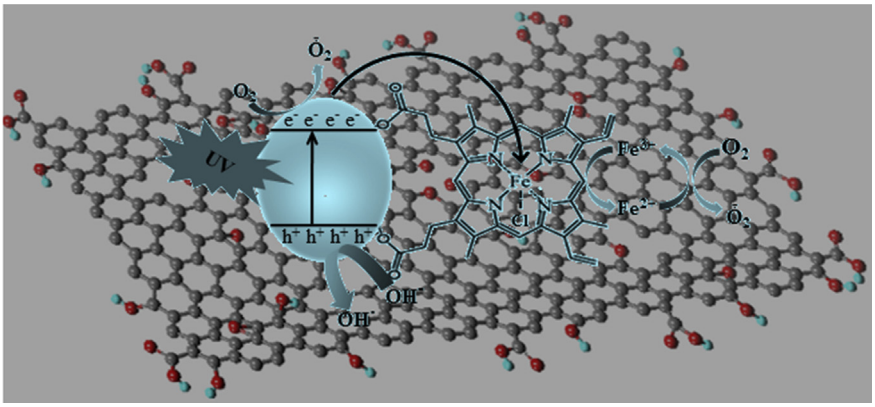

Scheme 4. The photogenerated electron – hole transfer from TiO_2/GO to Hemin to molecular oxygen.

TiO_2/GO electrons to enhance the photocatalytic activity. The band gap excitation produces a photo generated electron hole pair, the conduction band electron reduces the ferric Hemin to the ferrous Hemin and the valence band hole oxidizes the RhB dye molecules. The UV illumination took place after the ferric Hemin was quantitatively reduced to the ferrous Hemin [Scheme 4]. According to the crystal field theory, Fe^{2+} and Fe^{4+} ions are comparatively unstable compared to Fe^{3+} ions and hence detrap the electrons and holes to adsorb the molecular oxygen and the surface hydroxyl groups, respectively, to restore its half filled electronic configuration and thereby suppress the electron hole recombination. On the UV-visible light illumination, the photogenerated charge carriers are generated as shown the following Eqs. (10)–(12).

$$\text{Hemin-}TiO_2/GO(e^-) + Fe^{III}(\text{Hemin}) \rightarrow Fe^{II}(\text{Hemin})\ (\text{electron traping Hemin}) \quad (10)$$

$$\text{Hemin-}TiO_2/GO(e^-) + O_2 \rightarrow O_2^-\ (\text{electron traping oxygen}) \quad (11)$$

$$Fe^{II}(\text{Hemin}) + O_2 \rightarrow O_2^- + Fe^{III}(\text{Hemin})\ (\text{electron detraping}) \quad (12)$$

Due to the continuous cyclic process the ferric Hemin was quantitatively reduced to the ferrous Hemin in the presence of UV-visible light. The ferrous Hemin includes the source for the generation of hydroxyl radicals, thereby draws on the increase of the efficiency of the process. These hydroxyl radicals, the superoxide and the various other reactive oxygen species of graphene oxide can attack the chromophore of the dye molecules. Hemin serves as the electron transfer mediator playing the key role in the entire process of the photocatalytic degradation. The cleavage of the hydroxylase products is responsible for decolorization as shown in Scheme 2.

4. Conclusion

The GO-TiO_2-Hemin ternary hybrid composite was used as a photocatalyst in the photooxidative system for the degradation of the RhB in the presence of H_2O_2. The Hemin is anchored to the TiO_2 surface by the carboxylic group as confirmed by the FTIR technique. The system is found to be efficient under all pH conditions (ranging from 3 to 11). The mode of the Hemin molecule binding depends on the interfacial pH. The inner and outer sphere electron transfer process lead to the efficient degradation of the pollutant molecules. Based on their intermediates as analyzed by UV-visible spectroscopy and LC-MS techniques in the presented mechanism, a probable degradation pathway has been proposed. The proposed cyclic mechanism in which the iron-oxo species are formed by the MLCT along with the active hydroxyl radicals, positively enhanced the degradation rate immensely. Hence, the cyclic process sustains the reaction continuously. The results of this study suggest our photocatalyst approach can be photocatalyt considered as a novel, highly photocatalytic active, simple, safe, nontoxc, chemically stable and cost effective technology for the heterogeneous photocatalytic degradation of the RhB dyes using eco friendly TiO_2/GO/Hemin as a catalyst.

Acknowledgments

One of the authors, C. M. acknowledges the financial support from the Deparment of Science and Technology (DST) is greatful to DST- Science and Engineering Research Board (SERB) for the award of a National post Doctoral Fellowship (PDF/2017/001456) Government of India.

References

[1] C. Chen, W. Ma, J. Zhao, Photoelectrochemical properties of graphene and its derivaties, Chem. Soc. Rev. 39 (2010) 4206–4219.
[2] F. Chen, J. Zhao, H. Hidaka, Highly selective deethylation of Rhodamine B: adsorption and photooxidation pathways of the dye on the TiO_2/SnO_2 composite photocatalyst, Int. J. Photoenergy 5 (2003) 209–217.
[3] M.R. Hoffmann, S.T. Martin, W. Choi, D.W. Bahnemann, Environmental applications of semiconductor photocatalysis, Chem. Rev. 95 (1995) 69–96.
[4] O. Legrini, E. Oliveros, A.M. Braun, Photochemical processess for water treatment, J. Chem. Rev 93 (1993) 671–698.
[5] L. Gomathi Devi, S. Girish Kumar, K. Mohan Reddy, C. Munikrishnappa, Photo degradation of Methyl Orange an azo dye by Advanced Fenton Process using zero valent metallic iron: influence of various reaction parameters and its degradation mechanism, J. Hazard Mater. 164 (2009) 459–467.
[6] L. Gomathi Devi, S. Girish Kumar, K. Mohan Reddy, C. Munikrishnappa, Desalination and water treatment, Effect of various inorganic anions on the degradation of Congo red, a di azo dye, by the photo-assisted Fenton process using zero-valent metallic iron as a catalyst, Desalination Water Treat. 4 (2009) 294–305.
[7] D. Li, T. Yuranova, P. Albers, J. Kiwi, Accelerated Photobleaching of Orange II on novel ($H_5FeW_{12}O_{40}10H_2O$)/silica structured fabrics, J. Water Resour. 38 (2004) 3541–3550.
[8] S. Sabhi, J. Kiwi, S. Sabhi, J. Kiwi, Degradation of 2,4-Dichlorophenol by immobilized iron catalysts, J. Water Resour. 35 (8) (2001) 1994–2002.
[9] Samin Sardar, Prasenjit Kar, Samir Kumar Pal, The impact of central metal ions in Porphyrin functionalized ZnO/TiO_2 for enhanced solar energy conversion, J. Mat. Nano. Sci 1 (1) (2014) 12–30.
[10] Y. Li, X. Huang, Y. Li, Y. Xu, Y. Wang, e. Zhu, X. Duan, Y. Huang, Graphene-hemin hybrid material as effective catalyst for selective oxidation of primary C-H bond in toluene, J. Scientific reports 3 (2013) 1–7.
[11] Surender Kumar, S. Ghosh, N. Munichaindraiah, H.N. Vasan, 1.5 V battery driven reduced grapheme oxide-silver nanostructure coated carbon foam (rGO-Ag-CF) for the purification of drinking water, J. Nanotechnol. 24 (2013) 235101–235109.
[12] S.O. Obare, T. Ito, M.H. Balfour, G.J. Meyer, Ferrous hemin oxidation by organic halides at nanocrystalline TiO_2 interfaces, J. Nanoletters 3 (2003) 1151–1153.
[13] X. Lv, J. Weng, Ternary composite of hemin, gold nanoparticles and graphene for highly efficient decomposition of hydrogen peroxide, J. Nature Scientific. Rep. 3 (2013) 32851, 1-10.

[14] P.V. Kamat, Graphene-based nanoarchitectures. Anchoring semiconductor and metal nanoparticles on a two-dimensional carbon support, J. Phys. Chem. 1 (2010) 520–527.
[15] P.V. Kamat, Graphene-based nanoassemblies for energy conversion, J. Phys. Chem. Lett. 2 (2011) 242–251.
[16] T. Xue, S. Jiang, Y. Qu, Q. Su, R. Cheng, S. Dubin, C.Y. Chiu, R.B. Kaner, Y. Huang, X. Duan, Integration of molecular and enzymatic catalysts on graphene for biomimetic generation of antithrombotic species, J. Angew. Chem. Int. Ed 51 (2012) 3822–3825.
[17] W.S. Hummers Jr., R.E. Offeman, Preparation of graphitic oxide, J. Am. Chem. Soc. 80 (1958) 1339.
[18] L. Gomathi Devi, G.M. Krishnaiah, Photocatalytic degradation of p-amino-azo-benzene and p-hydroxy-azo-benzene using various heat treated TiO_2 as the photocatalyst, J. photochem. photobiol. A. Chem. 212 (1999) 141–145.
[19] Surender Kumar, C. Selvaraj, L.G. Scanlon, N. Munichandraiah, Ag nanoparticles-anchored reduced grapheme oxide catalyst for oxygen electrode reaction in aqueous electrolytes and also a non-aqueous electrolyte for Li-O2 cells, J. Phys. Chem. Phys 16 (2014) 22830–22840.
[20] E. Bae, W. Choi, Highly enhanced photoreductive degradation of perchlorinated compounds on dye-sensitized metal/TiO2 under visible light, Environ. Sci. Technol. 37 (2003) 147–152.
[21] K. Yu, S. Yang, H. He, C. Sun, C. Gu, Y. Ju, Visible light-driven photocatalytic degradation of Rhodamine B over NaBiO3: pathways and mechanism, J. Phys. Chem. A 113 (2009) 10024–10034.
[22] W.J. Wang, J.C. Yu, D.H. Xia, P.K. Wong, Y.C. Li, Graphene and g-C3N4 nanosheets cowrapped elemental alpha-sulfur as a novel metal-free heterojunction photocatalyst for bacterial inactivation under visible light, Environ. Sci. Technol. 47 (2013) 8724–8732.
[23] K. Dutta, S. Mukhopadhyay, S. Bhattacharjee, B. Chaudhuri, Chemical oxidation of methylene blue using a Fenton-like reaction, J. Hazard Mater. 84 (2001) 57–71.
[24] S. Girish Kumar, L. Gomathi Devi, Review on modified TiO2 photocatalysis under UV/visible light: selected results and related mechanisms on interfacial charge Carrier transfer dynamics, J. Phys. Chem. A 115 (2011) 13211–13241.
[25] C.E. Castro, R.S. Wade, Oxidation of Iron (II) porphyrins by alky halides, J. Am. Chem. Soc. 95 (1973) 226–234.
[26] C.E. Castro, R.S. Wade, N.O. Belser, biodehalogenation: reactions of cytochrome P-450 with polyhalomethanes, Biochemistry 24 (1985) 204–210.
[27] R.A. Larson, J.C. Silva, Dechlorination of substituted trichloromethanes by and Iron(III) porphyrin, J. Enviro. Toxicol. chem. 19 (2000) 543–548.
[28] Y. Huang, W. Ma, J. Li, M. Cheng, J. Zhao, A novel Beta-CD-hemin complex photocatalyst for efficient degradation of organic pollutants at neutral pHs under visible irradiation, J. Phys. Chem. B 107 (2003) 9409–9414.
[29] L. Gomathi Devi, L. Arunakumari, Enhanced photocatalytic performance of Hemin (chloro(protoporhyinato)iron(III)) anchored TiO_2 photocatalyst for methyl orange degradation: a surface modification method, Appl. Surf. Sci. 276 (2013) 521–528.